

Changing the colour of light in a silicon resonator

STEFAN F. PREBLE, QIANFAN XU AND MICHAL LIPSON*

School of Electrical and Computer Engineering, Cornell University, Ithaca, New York 14853, USA

*e-mail: lipson@ece.cornell.edu

Published online: 1 May 2007; doi:10.1038/nphoton.2007.72

As the demand for high bandwidths in microelectronic systems increases, optical interconnect architectures are now being considered that involve schemes commonly used in telecommunications, such as wavelength-division multiplexing (WDM) and wavelength conversion¹. In such on-chip architectures, the ability to perform wavelength conversion is required. So far wavelength conversion on a silicon chip has only been demonstrated using schemes that are fundamentally all-optical^{2–6}, making their integration on a microelectronic chip challenging. In contrast, we show wavelength conversion obtained by inducing ultrafast electro–optic tuning of a microcavity. It is well known that tuning the parameters of an optical cavity induces filtering of different colours of light⁷. Here we demonstrate that it can also change the colour of light. This is an effect often observed in other disciplines, for example, in acoustics, where the sound generated by a resonating guitar string can be modified by changing the length of the strings (that is, the resonators)⁸. Here we show this same tuning effect in optics, enabling compact on-chip electrical wavelength conversion. We demonstrate a change in wavelength of up to 2.5 nm with up to 34% on–off conversion efficiency.

Previous approaches to wavelength conversion on a silicon chip rely on nonlinear effects, such as cross-gain modulation, cross-phase modulation, cross-absorption modulation, four-wave mixing, difference-frequency generation^{2–5} or free-carrier effects⁶. However, all of these approaches have one thing in common—they are fundamentally all-optical, that is, they operate by imparting the optical signal carried by a high-intensity pump beam onto a probe beam. In contrast, in this work we show the feasibility of a new electro–optic approach to wavelength conversion that is based on dynamic cavity changes. The dynamic cavity change can be achieved by inducing small changes in refractive index in the cavity, either optically or electrically. Here we use the free-carrier plasma dispersion effect, an electro–optic effect, to induce the dynamic change in the cavity⁹, where the free-carrier concentration is induced using linear absorption of an optical pump. The same dispersion effect can also be induced electrically using a PIN diode, as recently demonstrated¹⁰, enabling the possibility of electrical wavelength conversion. The opto–optic experiment performed here gives a result that is equivalent to the one that would have been obtained if electrical injection of electrons and holes had been used.

We recently predicted that by dynamically tuning a resonator the wavelength of the light confined in the resonator would be changed¹¹. Notomi and Mitsugi showed that the physical effect

behind this wavelength conversion process is the adiabatic tuning of an oscillator, which is a classical linear phenomenon commonly observed in oscillators, such as a guitar string⁸. This effect was first investigated by Reed *et al.* in their theoretical studies of photonic crystals subjected to shock waves¹². In addition, it is also possible to stop light by similarly dynamically changing a coupled resonator system as was recently predicted by Yanik and Fan¹³.

The only requirement for the dynamic wavelength conversion process is that the resonator is modified in a timescale much shorter than the photon lifetime^{8,11,13}. Until recently, most on-chip resonators had a photon lifetime on the order of a picosecond, making it extremely difficult to meet this requirement for the wavelength-conversion process. However, we recently demonstrated the ultrafast tuning of compact silicon ring resonators with photon lifetimes of tens of picoseconds, making the work presented here possible^{14,15}. The cavity used here to change the frequency of incoming light is a silicon ring resonator of diameter 6 μm , with a waveguide cross-section of $0.45 \times 0.25 \mu\text{m}$, similar to the one in ref. 15. Unlike the resonator in ref. 15, we use an add/drop configuration here, where an additional waveguide is added adjacent to the ring, as seen in Fig. 1e. This additional waveguide is known as the drop port. The ring resonator is measured to have a free spectral range of 29.1 nm, corresponding to a group index of $n_g = 4.45$ (ref. 16). The quality factor, Q , is $\cong \lambda_0 / \Delta\lambda_{\text{FWHM}} = 18,614$, where $\lambda_0 = 1,564.3 \text{ nm}$ is the resonance wavelength and $\Delta\lambda_{\text{FWHM}} = 0.084 \text{ nm}$ is the resonance full width at half maximum (FWHM). This Q -factor corresponds to a photon lifetime of $\tau_{\text{ph}} = \lambda_0^2 / (2\pi c \Delta\lambda_{\text{FWHM}}) = 15.5 \text{ ps}$, where c is the speed of light in vacuum¹⁵.

In order to induce a fast dynamic change in the resonator, we induce a refractive-index change using free-carrier injection. The carrier concentration is induced using short optical pump pulses; however, the injection of carriers can also be induced electrically¹⁰. As seen in Fig. 2, the optical pump is incident on the top of the ring resonator and is linearly absorbed, which generates free carriers. The free carriers cause a reduction in the ring's refractive index, which in turn causes the resonator's resonance to blue shift^{9,15}. This resonance shift causes the wavelength of the probe light confined in the resonator also to blue-shift by the same amount, as depicted in Fig. 1e.

In order to show the effect of the cavity on wavelength conversion, in Fig. 1a–d we show the normalized probe transmission for four different detunings (indicated as a–d on

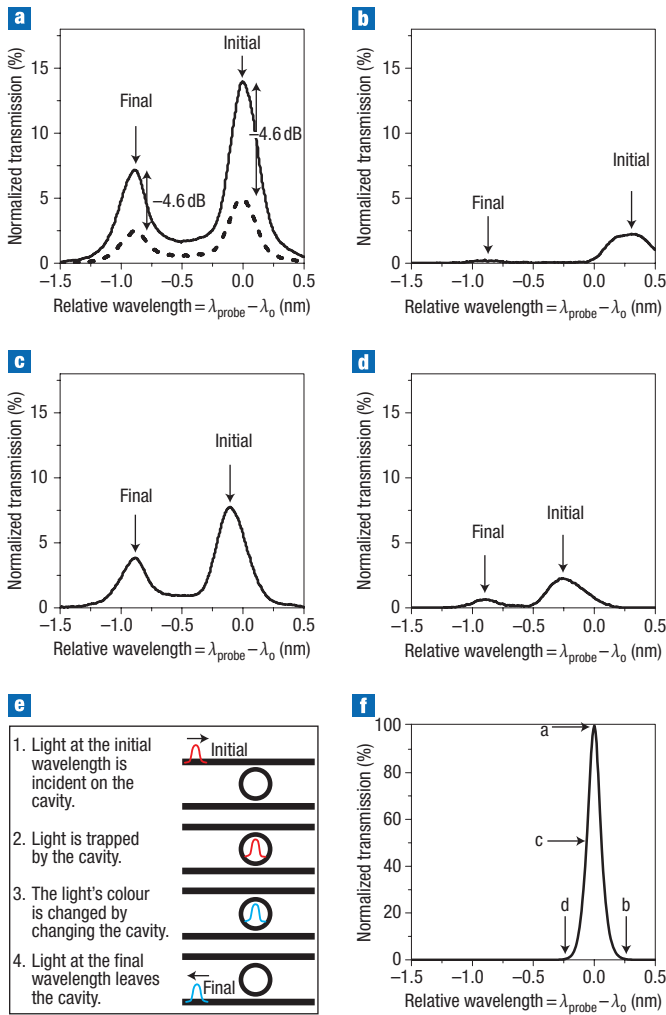


Figure 1 Wavelength conversion dependence on cavity detuning. **a–d**, Transmission spectra for four different detunings of the incident probe light wavelength relative to the cavity mode. Maximum conversion occurs when the probe is tuned to be on resonance, the dashed line is when the probe input power is reduced by 4.6 dB (**a**). The final wavelength is determined only by the degree of dynamic cavity change. **e**, Illustration of the wavelength-conversion process. **f**, The peak transmission of the probe when the pump is off. The four initial probe wavelengths (**a–d**) are indicated.

Fig. 1f) of the incident probe-light wavelength relative to the initial cavity mode, $\lambda_{\text{probe}} - \lambda_0$, where the pump energy is fixed. The probe transmission is normalized to the peak transmission of the probe when the pump is off (shown in Fig. 1f). When the probe is in resonance or close to resonance with the cavity mode (Fig. 1a and c, respectively), a high degree of light is converted from the initial to the final wavelength. When the initial wavelength of the probe is detuned from the resonance (seen in Fig. 1b and d) very little light is converted, because very little is initially coupled into the resonator. It can be seen that the final wavelength is fixed in all of these cases and is consequently independent of the initial one. This is because the converted wavelength is determined only by the final state of the resonator, which is fixed because the pump energy is fixed in these four examples. In addition, we verified that the final wavelength was in fact the same as the final state of the resonator using a temporally delayed probe pulse.

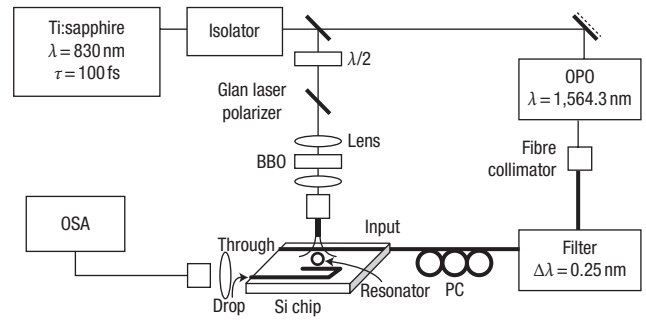


Figure 2 Experimental set-up used to measure the wavelength-conversion process. OSA, optical spectrum analyser; PC, polarization controller; OPO, optical parametric oscillator; BBO, beta-barium borate crystal. The pump (illuminating the top of the resonator) is used to induce a dynamic change in the cavity, while the probe light (supplied by the OPO) is confined in the ring resonator.

It is also shown in Fig. 1a (dashed line) that when the probe input power is reduced by 4.6 dB, the measured transmitted probe signal is also reduced by the same amount and is otherwise unchanged, indicating that the probe itself does not induce any nonlinearities. Note also that the ratio of the light at the final wavelength and at the initial cavity mode ($\lambda = \lambda_0$) is constant for all detunings, as is expected. This can be seen in Fig. 1a and c. Note that in Fig. 1b and d, where the initial wavelength is not the same, because most of the light seen at the initial wavelength is not coupled to the cavity mode in these cases.

In contrast to other processes demonstrated so far for wavelength conversion, such as Raman-based⁵ and four-wave mixing^{2–4}, the change in wavelength is solely dependent on the pump intensity and not on the pump or probe wavelengths. This is because the wavelength change is determined solely by the resonance tuning of the ring^{8,11}, which is controlled by the injected free-carrier concentration. In Fig. 3 we show the linear dependence of wavelength change with the absorbed pump energy (filled squares, measured; solid line, linear fit). The insets show the probe power versus wavelength relative to the initial cavity resonance for absorbed pump energies of 0.419 pJ (Fig. 3a) and 1.38 pJ (Fig. 3b). Note that the absorbed pump energy is approximately 7% of the incident pump light, owing to the small overlap of the pump beam (spot-size diameter of approximately 10 μm) and ring area. This is not a fundamental limitation and can be solved using an in-plane pumping scheme, as used previously by our group¹⁴. The slope of the fitted line is equal to 1.75 nm pJ⁻¹, in close agreement with the theoretical value of $\lambda_0 C_N \lambda_{\text{pump}} / (n_e h c V) = 1.67 \text{ nm pJ}^{-1}$, where $C_N = 3 \times 10^{-21} \text{ cm}^3$ is the approximate free-carrier plasma-effect coefficient⁹, λ_{pump} is the pump wavelength, $n_e = 2.4$ is the resonator's effective index¹⁷, h is Planck's constant and V is the volume of the ring.

The experimental on–off conversion efficiency is plotted in Fig. 4 (squares) as a function of wavelength change. We define the conversion efficiency as $\eta = 100 P(\lambda_{\text{final}}) / P_{\text{off}}(\lambda_0) \cdot \Delta\lambda_{\text{final}} / \Delta\lambda_0$ where λ_{final} is the final wavelength, $P(\lambda_{\text{final}})$ is the peak probe power at the final wavelength, $P_{\text{off}}(\lambda_0)$ is the transmitted peak probe power when the pump is off (seen in Fig. 1f), $\Delta\lambda_{\text{final}}$ is the FWHM of the probe signal at the final wavelength, and $\Delta\lambda_0$ is the probe FWHM when the pump is off. Note that the FWHMs are included in the efficiency calculation

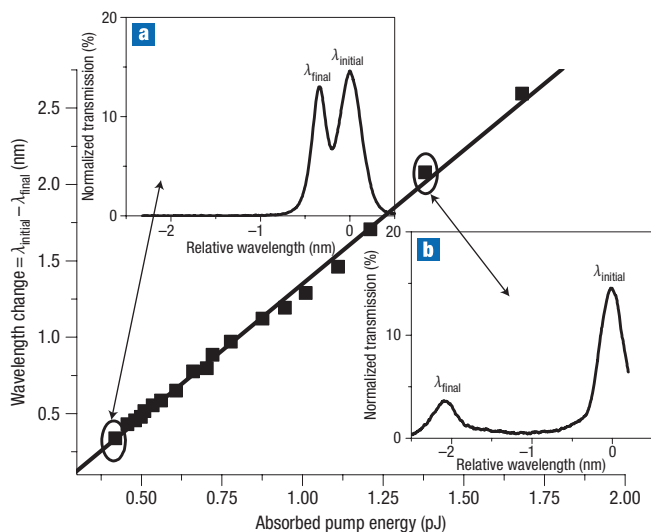


Figure 3 Dependence of the measured wavelength change on the absorbed pump energy. (Squares, measured; solid line, linear fit) **a,b**, The insets show the transmitted probe power against wavelength relative to the initial cavity resonance for absorbed pump energies of 0.419 pJ (upper-left inset, $\lambda_{\text{initial}} - \lambda_{\text{final}} = 0.339$ nm, induced carrier concentration $\Delta N = 1.65 \times 10^{17} \text{ cm}^{-3}$) and 1.38 pJ (lower-right inset, $\lambda_{\text{initial}} - \lambda_{\text{final}} = 2.08$ nm, induced carrier concentration $\Delta N = 1.39 \times 10^{18} \text{ cm}^{-3}$), respectively.

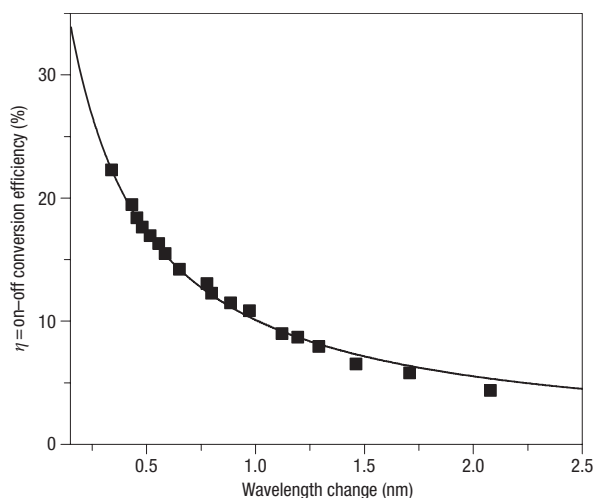


Figure 4 On-off conversion efficiency dependence on wavelength change. The solid line shows our theoretical calculations and the squares our experimental conversion-efficiency results. The maximum conversion efficiency (34%) was extrapolated from a fit of the experimental data. Free-carrier absorption reduces the conversion efficiency for increasing wavelength changes.

because the bandwidth of the light changes slightly when the pump is on. It is seen that the conversion efficiency decreases as the wavelength change increases, and correspondingly as the pump power increases (also seen in the insets of Fig. 3). This is because as more free carriers are generated, more of the light at the final wavelength is absorbed⁹. This is confirmed by calculating the theoretical efficiency (solid line in Fig. 4) as given by $\eta = \eta_o \cdot Q_{\text{pump}}/Q_{\text{no-pump}}$, where $Q_{\text{pump}} = \pi n_g/\lambda_0 \alpha$ is the cavity's quality

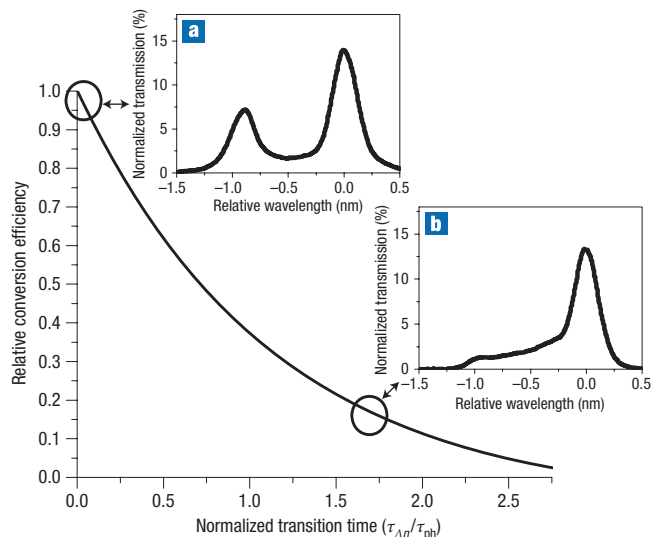


Figure 5 Relative conversion efficiency as a function of the cavity's transition time from its initial to final states. The transition time is normalized to the photon lifetime of the cavity. The solid line is an exponential decay fit to data calculated using two-dimensional FDTD simulations. **a,b**, The insets show the measured probe power with two different pump-pulse durations (cavity transition times).

factor in the presence of free carriers⁶, $Q_{\text{no-pump}} = 18,614$ is the quality factor with no pump, and $\eta_o = 34\%$ is a fitting parameter verified using finite-difference time-domain (FDTD) simulations. The variable α is the roundtrip loss in the ring resonator and is given by $\alpha = \alpha_{\text{no-pump}} + \alpha_{\text{pump}}$, where $\alpha_{\text{no-pump}} = 4.81 \text{ cm}^{-1}$ is the inherent loss of the ring and $\alpha_{\text{pump}} = (14.5 \times 10^{-18}) \cdot \Delta N [\text{cm}^{-1}] = (14.5 \times 10^{-18}) \cdot E_{\text{pump}} \lambda_{\text{pump}} / (hcV) [\text{cm}^{-1}]$ is the loss induced by the free carriers, where $E_{\text{pump}} = (\lambda_{\text{initial}} - \lambda_{\text{final}}) / 1.75$ [pJ] is the absorbed pump energy^{9,17}. λ_{initial} is the initial wavelength and ΔN is the induced carrier concentration.

The maximum on-off conversion efficiency achieved here is approximately 34%. It was previously determined that the theoretical efficiency should be close to 100% (refs 8 and 11). However, this is only the efficiency for the light that is in the resonator during the conversion process. The discrepancy arises because, in reality, not all of the probe pulse is in the resonator when the conversion process occurs. Some of the light at the leading edge of the probe pulse leaks out of the ring before the conversion process begins, which is clearly seen as the light at the initial wavelength in Fig. 1a (and in the insets of Fig. 3). In addition, the light at the trailing edge of the probe pulse, which has not yet entered the ring resonator when the conversion occurs, cannot be converted because the ring resonator is now not on resonance with that light. This problem was recently addressed by Gaburro and colleagues, who proposed a solution based on a coupled resonator waveguide in order to ensure a larger portion of the probe pulse is in the system during the conversion¹⁸. We also determined the overall conversion efficiency per pulse at the drop port to be approximately 5.8%. If the light coupled out of the through port is also taken into account, the total efficiency coupled out of the resonator is 11.6%. Note that this efficiency can be considerably increased, because in the current experimental set-up, the bandwidth of the probe (0.25 nm) is much larger than the bandwidth of the cavity (0.084 nm).

In order to ensure a high conversion efficiency, the transition from the cavity initial state to final state (in our case determined by the pump pulse duration) must be fast enough, in fact while the probe pulse is trapped in the cavity¹¹. This is seen in Fig. 5, where the relative conversion efficiency as a function of the cavity's transition time from its initial state to its final state (normalized to the lifetime of the cavity) is plotted. The curve was calculated using FDTD simulations. One can see that the e^{-1} point of the curve is approximately at the point where the index change time is equal to the photon lifetime, as expected. In the inset we show two experimental transmission spectra, one where the pump pulse is sent through a short 25-cm piece of SMF-28 fibre (Fig. 5a), and another obtained by sending the pump through 3.5 m of fibre in order to lengthen the duration of the pump pulse to be of the order of the photon lifetime of the cavity (Fig. 5b). In the latter case it is seen that there is significantly less light at the final state, and it is spread out from the initial to the final state of the resonator because the light is continuously leaking out during the slow conversion process. Thus, in order to obtain a significant power conversion at the final wavelength in this device, the cavity change needs to occur in a timescale less than 10 ps. This requirement can be relaxed when using a higher- Q cavity^{19,20}. Note that in this work, the Q value of the device does decrease slightly due to free-carrier absorption^{6,9,16}. However, it never reduces sufficiently for the cavity transition used here (100 fs) to be too slow.

In conclusion, we demonstrated the feasibility of electro-optic wavelength conversion using the ultrafast dynamic tuning of a resonant cavity with the injection of free carriers. Here, optical injection was used, but in future, carriers could be injected or extracted on the required timescales using the recently demonstrated PIN diode electro-optic modulators^{17,21}. This work could open the door to a chip-based WDM system, where a large range of wavelengths could be generated from a single light source at a single wavelength. The ability to dynamically tune the properties of a resonator could also enable the stopping of light, as was suggested recently by Yanik and Fan¹³. Note that in this work, free-carrier absorption limits conversion efficiency as the wavelength change increases. In future devices, this absorption loss could be counteracted by gain or by extracting the carriers using a reverse-biased diode^{3,17,22}.

METHODS

The experimental set-up is depicted in Fig. 2. The pump source is a mode-locked Ti:sapphire laser that generates 100-fs pulses at 830 nm, with 5 nJ of energy, at an $R_{\text{pump}} = 76.47$ MHz repetition rate. A beta-barium-borate (BBO) crystal is used to generate second-harmonic pulses centred at $\lambda_{\text{pump}} = 415$ nm. At this wavelength, the strong linear absorption in silicon causes 90% of the photons transmitted into the 250-nm-thick silicon layer to be absorbed¹⁵. After second harmonic generation, the pump pulses are coupled into a short (less than 25 cm) SMF-28 fibre and then exit the output facet, which is placed close to the top surface of the resonator. The energy of the pulse incident on the ring resonator plane is less than 25 pJ. The Ti:sapphire also pumps an optical parametric oscillator, which produces the probe pulses. The probe pulses are passed through

a $\Delta\lambda = 0.25$ nm filter (pulse duration measured and theoretically calculated to be approximately $\tau_{\Delta\lambda} = 18$ ps), then polarized and coupled into the silicon waveguide by an external tapered-lens fibre and an on-chip fibre-to-waveguide nanotaper coupler¹⁵. The quasi-TE (transverse electric; chosen over quasi-TM, transverse magnetic, due to its higher Q) light coupled into the ring resonator's drop port is then coupled into a fibre by a lens/collimator and detected by an optical spectrum analyser. The pump and probe pulses are aligned in time so that the leading edge of the pump's pulse occurs when probe amplitude in the resonator is at a maximum.

Received 17 January 2007; accepted 23 March 2007; published 1 May 2007.

References

1. Yoo, S. J. B. Wavelength conversion technologies for WDM network applications. *J. Lightwave Technol.* **14**, 955–966 (1996).
2. Espinola, R. L., Dadap, J. L., Osgood, R. M. Jr, McNab, S. J. & Vlasov, Y. A. C-band wavelength conversion in silicon photonic wire waveguides. *Opt. Express* **13**, 4341–4349 (2005).
3. Foster, M. A. *et al.* Broad-band optical parametric gain on a silicon photonic chip. *Nature* **441**, 960–963 (2006).
4. Fukuda, H. *et al.* Four-wave mixing in silicon wire waveguides. *Opt. Express* **13**, 4629–4637 (2005).
5. Jalali, B., Raghunathan, V., Dimitropoulos, D. & Boyraz, O. Raman-based silicon photonics. *IEEE J. Sel. Top. Quant. Electron.* **12**, 412–421 (2006).
6. Xu, Q., Almeida, V. R. & Lipson, M. Micrometer-scale all-optical wavelength converter on silicon. *Opt. Lett.* **30**, 2733–2735 (2005).
7. Vahala, K. J. Optical microcavities. *Nature* **424**, 839–846 (2003).
8. Notomi, M. & Mitsugi, S. Wavelength conversion via dynamic refractive index tuning of a cavity. *Phys. Rev. A* **73**, 051803 (2006).
9. Soref, R. A. & Bennett, B. R. Kramers–Kronig analysis of electro-optical switching in silicon. *SPIE Integr. Opt. Circuit Eng.* **704**, 32–37 (1987).
10. Xu, Q., Schmidt, B., Pradhan, S. & Lipson, M. Micrometer-scale silicon electro-optic modulator. *Nature* **435**, 325–327 (2005).
11. Preble, S. F. & Lipson, M. Conversion of a signal wavelength in a dynamically tuned resonator. *Integrated Photonics Research and Applications Topical Meeting, IMC5* (2006).
12. Reed, E. J., Soljacic, M. & Joannopoulos, J. D. Color of shock waves in photonic crystals. *Phys. Rev. Lett.* **90**, 203904 (2003).
13. Yanik, M. F. & Fan, S. Dynamic photonic structures: stopping, storage, and time reversal of light. *Studies Appl. Math.* **115**, 233–253 (2005).
14. Almeida, V. R., Barrios, C. A., Panepucci, R. R. & Lipson, M. All-optical control of light on a silicon chip. *Nature* **431**, 1081–1084 (2004).
15. Almeida, V. R. *et al.* All-optical switching on a silicon chip. *Opt. Lett.* **29**, 2867–2869 (2004).
16. Yariv, A. Universal relations for coupling of optical power between microresonators and dielectric waveguides. *Electron. Lett.* **36**, 321–322 (2000).
17. Preble, S. F., Xu, Q., Schmidt, B. S. & Lipson, M. Ultrafast all-optical modulation on a silicon chip. *Opt. Lett.* **30**, 2891–2893 (2005).
18. Gaburro, Z. *et al.* Photon energy lifter. *Opt. Express* **14**, 7270–7278 (2006).
19. Loncar, M., Hochberg, M., Scherer, A. & Yüeming, Q. High quality factors and room-temperature lasing in a modified single-defect photonic crystal cavity. *Opt. Lett.* **29**, 721–723 (2004).
20. Song, B.-S., Noda, S., Asano, T. & Akahane, Y. Ultra-high- Q photonic double-heterostructure nanocavity. *Nature Mater.* **4**, 207–210 (2005).
21. Xu, Q., Manipatruni, S., Schmidt, B., Shakya, J. & Lipson, M. 12.5 Gbit/s carrier-injection-based silicon micro-ring silicon modulators. *Opt. Express* **15**, 430–436 (2007).
22. Rong, H. *et al.* A continuous-wave Raman silicon laser. *Nature* **433**, 725–728 (2005).

Acknowledgements

The authors acknowledge support by the Center for Nanoscale Systems, supported by the National Science Foundation. We thank Gernot Pomrenke from the Air Force Office of Scientific Research (AFOSR) for partially supporting this work. This work was performed in part at the Cornell Nano-Science & Technology Facility (a member of the National Nanofabrication Users Network), which is supported by the National Science Foundation, its users, Cornell University and Industrial Affiliates. Correspondence and requests for materials should be addressed to M.L.

Author contributions

S.F.P. conceived the idea, performed measurements and drafted the manuscript. Q.X. supported discussion. M.L. contributed to the manuscript.

Competing financial interests

The authors declare no competing financial interests.

Reprints and permission information is available online at <http://npg.nature.com/reprintsandpermissions/>